DOI: 10.1002/ange.201306083

Hydrogen Storage

Immobilization of Aluminum Borohydride Hexammoniate in a Nanoporous Polymer Stabilizer for Enhanced Chemical Hydrogen Storage**

Ziwei Tang, Yingbin Tan, Xiaowei Chen, Liuzhang Ouyang, Min Zhu, Dalin Sun, and Xuebin Yu**

With global warming and environmental pollution worsening, the search for alternative fuels is a matter of great importance. Hydrogen is an excellent energy-storage medium because of its abundance, high chemical energy, and low-emission combustion. However, hydrogen remains underutilized as a fuel source because of a lack of storage capacity.[1] Recently, considerable efforts have been directed towards light-weight metal hydrides[2] and chemical hydrides.[3] Among them, metal borohydrides ($M(BH_4)_m$, MBs) have attracted significant interest because of their high theoretical hydrogen content. Unfortunately, the use of MBs in portable power sources is limited by the poor thermodynamic and kinetic properties of hydrogen release.[4] Recently, we have adopted an efficient strategy that introduces $H^{\delta+}$ to MBs by NH_3 coordination and results in the formation of metal borohydride ammoniates (MBAs, $M(BH_4)_m{\cdot}n\,NH_3$).[5] Thus, interactions between $H^{\delta+}$ and $H^{\delta-}$ become feasible, and hydrogen release is promoted at much lower temperatures. Among the known MBAs, $Al(BH_4)_3{\cdot}6\,NH_3$ features a comparatively high hydrogen capacity (17.4 wt%), high stability in air, and other properties that favor dehydrogenation.[5a] Nevertheless, this process is hampered by slow dehydrogenation kinetics at moderate temperatures, simultaneous release of ammonia upon thermolysis, and poor reversibility of dehydrogenation reactions; these challenges markedly limit portable power applications of this MBA.

General methods for enhancing hydrogen-storage properties of chemical hydrides include the addition of additives[6] or catalysts[7] to modify their dehydrogenation thermodynamics, improve the kinetics, and depress the release of undesirable gases. Thus far, these approaches have led to significant advances of many attractive hydrides.[8] Recently, nanoconfinement has offered new insights and solutions to current hydrogen-storage technology.[9] Theoretical calculations and preliminary experiments have shown that nanoconfined hydrides feature a significantly improved hydrogen-storage performance with respect to their bulk counterparts.[10] Two routes have been widely used to encapsulate hydrogen-storage materials into nanoscaffolds: solution impregnation and melt infiltration.[11] However, most MBAs, including $Al(BH_4)_3{\cdot}6\,NH_3$, have neither a melting point that is lower than the decomposition temperature, nor solubility in a common organic solvent; thus it is difficult to achieve size-confinement of this class of materials with either of these known approaches. Therefore, a new two-step procedure is proposed in which the stabilization of the MB is first realized within a nanosupport; this is followed by a treatment with gaseous ammonia to produce the targeted MBA/support nanocomposite.

Herein, we report the successful synthesis of nanoconfined $Al(BH_4)_3{\cdot}6\,NH_3$. As $Al(BH_4)_3$ is volatile and unstable under ambient conditions, its capture in a nanosupport is difficult to achieve by commonly used approaches. The poly(styrene-*co*-divinylbenzene) (PSDB) resin, a hypercross-linked porous polymer, was employed as the nanosupport in this study. The phenyl ring of the PSDB resin (Supporting Information, Figure S1) can interact with the Lewis acidic metal cations,[12] such as Al^{3+} in $Al(BH_4)_3$, which leads to the anchoring of the cations. Subsequent treatment with ammonia yields well-distributed $Al(BH_4)_3{\cdot}6\,NH_3$ (Figure 1).

The immobilization process was monitored by NMR spectroscopy. Interaction of $Al(BH_4)_3$ with the PSDB resin is indicated by solid-state NMR measurements (Figure 1b; Supporting Information, Figures S2 and S3). The ^{27}Al NMR spectrum shows a sharp peak at 5.7 ppm, which is similar to that of $Al(BH_4)_3{\cdot}NMe_3$ (Supporting Information, Figure S2). These peaks suggest that the phenyl rings of PSDB play a role in stabilizing the $Al(BH_4)_3$ molecules by coordinating to the aluminum atoms, similar to the formation of the adduct $Al(BH_4)_3{\leftarrow}NMe_3$, which contains a seven-coordinate aluminum center (one NMe_3 ligand and six bridging hydrogen atoms).[13] Density functional theory (DFT) calculations further illustrate the interactions between the initially introduced $Al(BH_4)_3$ molecules and the phenyl rings in $Al(BH_4)_3$/

[*] Z. Tang, Y. Tan, X. Chen, Prof. D. Sun, Prof. X. Yu
Department of Materials Science, Fudan University
Shanghai, 200433 (P.R. China)
E-mail: yuxuebin@fudan.edu.cn
Prof. L. Ouyang, Prof. M. Zhu
School of Materials Science and Engineering
South China University of Technology
Guangzhou, 510641 (P.R. China)
E-mail: memzhu@scut.edu.cn

[**] We gratefully acknowledge enlightening suggestions and elaborative amendments to this paper by a reviewer, and financial support from the Ministry of Science and Technology of China (2010CB631302), the National Natural Science Foundation of China (51071047, 21271046, and 51271078), the Ph.D. Programs Foundation of the Ministry of Education of China (20110071110009), and the Science and Technology Commission of Shanghai Municipality (11JC1400700 and 11520701100).

Supporting information for this article is available on the WWW under http://dx.doi.org/10.1002/anie.201306083.

 © 2013 Wiley-VCH Verlag GmbH & Co. KGaA, Weinheim

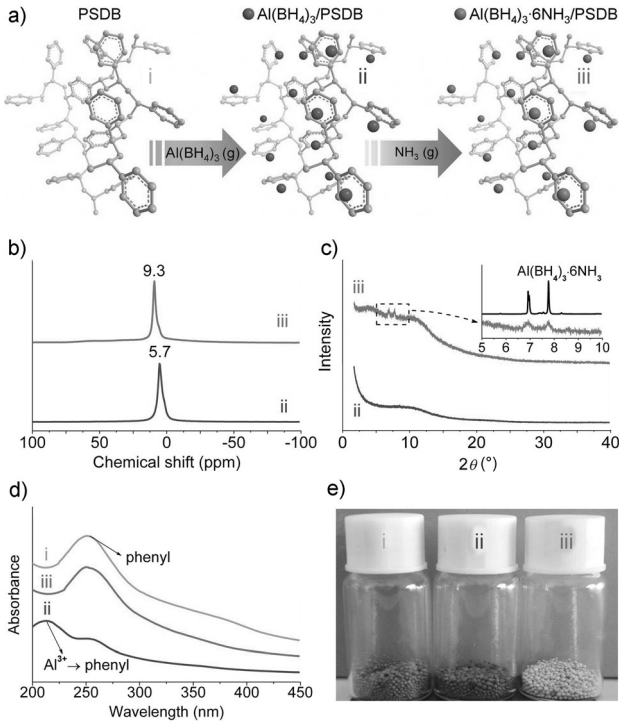

Figure 1. a) Formation of the $Al(BH_4)_3{\cdot}6NH_3$/PSDB composite (iii) from the $Al(BH_4)_3$/PSDB composite (ii), which was obtained from a PSDB resin (i). b) Solid-state ^{27}Al NMR spectra of (ii) and (iii). c) HRXRD patterns of (ii) and (iii); inset: zoom-in image of the regional XRD patterns of $Al(BH_4)_3{\cdot}6NH_3$/PSDB compared with that of bulk $Al(BH_4)_3{\cdot}6NH_3$. d) UV absorption spectra of (i), (ii), and (iii). e) Photograph showing samples of (i), (ii), and (iii).

PSDB, which guarantee a uniform dispersion of $Al(BH_4)_3$ in the PSDB resin (Supporting Information, Figure S4). Although validation of successful loading with $Al(BH_4)_3$ is difficult because of the amorphous state of $Al(BH_4)_3$/PSDB, which was observed by high-resolution X-ray diffraction (HRXRD; Figure 1c), the formation of the $Al(BH_4)_3{\cdot}6NH_3$/PSDB composite was confirmed by the detection of peaks characteristic of $Al(BH_4)_3{\cdot}6NH_3$. This was further affirmed by the ^{11}B NMR (Supporting Information, Figure S3) and (Figure 1b) of $Al(BH_4)_3{\cdot}6NH_3$/PSDB; for this composite, a peak at 9.3 ppm in the ^{27}Al NMR spectrum was assigned to the aluminum atom that is coordinated by six nitrogen atoms, which is consistent with that of bulk $Al(BH_4)_3{\cdot}6NH_3$.[5a]

The UV absorption of the PSDB resin varied during the procedure (Figure 1d). The absorption band centered at 251 nm is attributed to the phenyl π–π* electron transitions of PSDB.[12d] Once $Al(BH_4)_3$ had been incorporated, the intensity of that absorption band notably decreased, while a new peak was observed at 212 nm; this peak is due to the interaction of Al^{3+} with the phenyl ring. This interaction also led to an apparent color change of PSDB (Figure 1e). After the coordination of the NH_3 ligands to the aluminum center, which led to the formation of $Al(BH_4)_3{\cdot}6NH_3$, the UV absorption spectrum of the $Al(BH_4)_3{\cdot}6NH_3$/PSDB composite showed a similar absorption band as the PSDB resin, which indicates that there were no further interactions between Al^{3+} and the PSDB resin. As a result, the colorless PSDB composite ((iii), Figure 1e) now reflects the loading of $Al(BH_4)_3{\cdot}6NH_3$. This process was further elucidated by DFT calculations (Supporting Information, Figure S5), which revealed a decrease in the binding energy between $Al(BH_4)_3{\cdot}6NH_3$ and PSDB compared to that of $Al(BH_4)_3$ and PSDB.

Elemental analysis (Al, B, N, H) of the $Al(BH_4)_3{\cdot}6NH_3$/PSDB composite demonstrated that $Al(BH_4)_3$ was fully transformed into its hexammoniate, and also revealed the amount of $Al(BH_4)_3{\cdot}6NH_3$ in the composite (up to 37.3 wt%). This value is much higher than that for other scaffolds, including porous carbon, that were loaded with $Al(BH_4)_3{\cdot}6NH_3$ by the same route, which indicates the obvious advantage of the PSDB resin in facilitating this process. By combining the measured densities and the pore volume of the composites (Supporting Information, Figure S6), the loading capacity of $Al(BH_4)_3{\cdot}6NH_3$ inside the pores of the PSDB was calculated to be 30.7 wt% (for detailed calculations, see the Supporting Information).

A scanning electron microscope (SEM) image of the PSDB resin reveals a typical nanoporous structure (Figure 2a), whereas a significant decrease in porosity is seen for both the $Al(BH_4)_3$/PSDB and $Al(BH_4)_3{\cdot}6NH_3$/PSDB composites (Figure 2b,c). Further morphological examination of the nanosupport by transmission electron microscopy (TEM) clearly showed the cross-linked porous network of the PSDB resin (Figure 2d); a pore-diameter distribution of 10–100 nm is visible. $Al(BH_4)_3$ and $Al(BH_4)_3{\cdot}6NH_3$ that were embedded within the matrix are shown in Figure 2e,f. In the energy-dispersive spectroscopic (EDS) analysis of the two composites (Supporting Information, Figure S7), the detection of

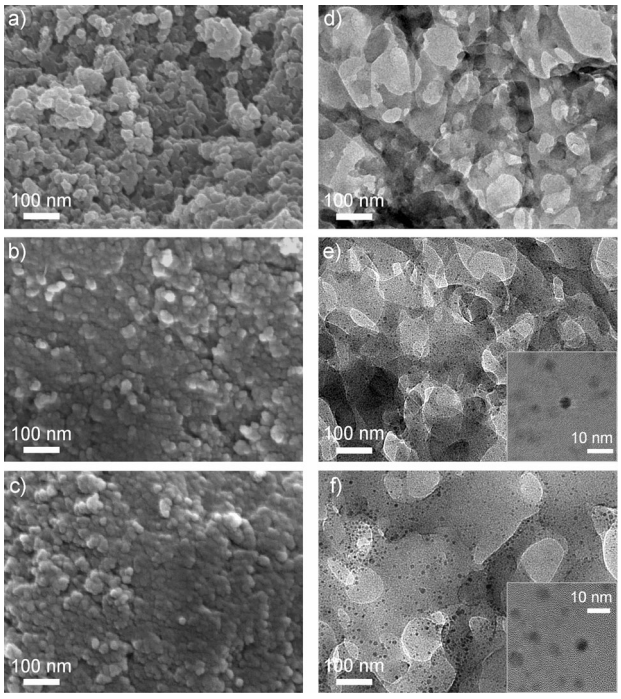

Figure 2. SEM (a–c) and TEM micrographs (d–f) of the PSDB resin and the $Al(BH_4)_3$/PSDB and $Al(BH_4)_3{\cdot}6NH_3$/PSDB composites, respectively; the insets show the corresponding HRTEM micrographs.

© 2013 Wiley-VCH Verlag GmbH & Co. KGaA, Weinheim

aluminum also implied the successful encapsulation of the two hydrides into the PSDB resin. Even though the composites had a high loading of hydrides, a uniform distribution of the nanoparticles (which resulted from subsequent aggregation of multiple $Al(BH_4)_3$/$Al(BH_4)_3{\cdot}6NH_3$ molecules) with average diameters of approximately 4 and 7 nm is observed by high-resolution TEM (HRTEM) of $Al(BH_4)_3$/PSDB (Figure 2e, inset) and $Al(BH_4)_3{\cdot}6NH_3$/PSDB (Figure 2f, inset; the corresponding zoom-in images are shown in Figure S8). These results all suggest a superior size-controlling effect of the PSDB resin on MB and MBA materials.

The onset of dehydrogenation and the peak temperature of $Al(BH_4)_3{\cdot}6NH_3$ are lowered from 140 to 67 °C, and from 175 to 121 °C, respectively, after encapsulation within the PSDB resin (Figure 3a). Moreover, the NH_3 signals in the mass spectrum (MS), and the calculated purity of H_2 that was obtained from thermal gravimetry (TG) and volumetric temperature-programmed desorption (TPD; Supporting Information, Figure S9) tests reveal a satisfactory depression of ammonia liberation from the nanocomposite compared to that of the bulk material (Supporting Information, Table S1).

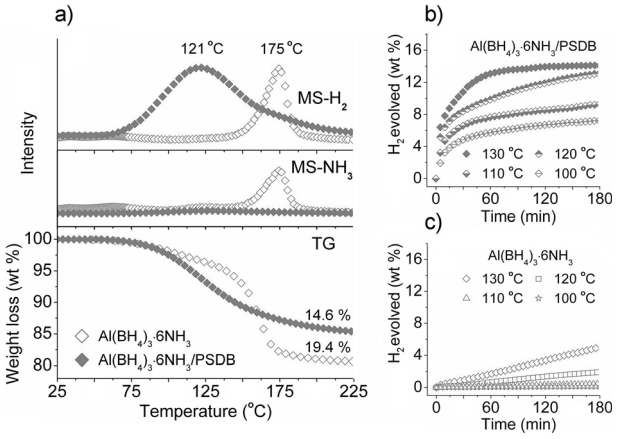

Figure 3. a) MS and TG profiles of $Al(BH_4)_3{\cdot}6NH_3$/PSDB and bulk $Al(BH_4)_3{\cdot}6NH_3$ with a heating rate of 5 °C min^{-1}. Isothermal TPD results of hydrogen released from $Al(BH_4)_3{\cdot}6NH_3$/PSDB (b) and bulk $Al(BH_4)_3{\cdot}6NH_3$ (c) at 100, 110, 120, and 130 °C (PSDB was not considered as a gravimetric component in the measurements).

The advanced dehydrogenation performance of PSDB-confined $Al(BH_4)_3{\cdot}6NH_3$ is further demonstrated by isothermal desorption, which was measured at various temperatures. PSDB-confined $Al(BH_4)_3{\cdot}6NH_3$ (Figure 3b) can release more than 10 wt % of hydrogen in less than 30 min, and the maximum hydrogen-release capacity (ca. 14 wt %, corresponding to 5.2 wt % relative to the whole system) was reached within two hours at 130 °C. Even at 120 °C, more than 10 wt % of hydrogen can be evolved within 1 h. When heating at 100 °C, hydrogen evolution of about 7.2 wt % is achieved within 3 h with $Al(BH_4)_3{\cdot}6NH_3$/PSDB, whereas only 4.9 wt % of hydrogen is released from bulk $Al(BH_4)_3{\cdot}6NH_3$ in the same period of time, even at 130 °C (Figure 3c). After incorporation within the PSDB resin, the apparent activation energy of H_2 liberation from $Al(BH_4)_3{\cdot}6NH_3$ was decreased from 118.1 to 53.2 kJ mol^{-1} (Supporting Information, Figure S10). To verify the possible templating effect that results from the randomly distributed phenyl rings in PSDB, a sample of $Al(BH_4)_3{\cdot}6NH_3$ (37 wt %) was prepared by ball milling with PSDB. The TPD result (Supporting Information, Figure S11) indicated a positive effect of templating on the solid-state dehydrogenation process. Therefore, significantly enhanced dehydrogenation of $Al(BH_4)_3{\cdot}6NH_3$ incorporated into PSDB can be attributed to both size control and a templating effect from the randomly distributed phenyl rings.

The FTIR spectrum of $Al(BH_4)_3{\cdot}6NH_3$/PSDB includes peaks that are due to $Al(BH_4)_3{\cdot}6NH_3$ and the PSDB resin. Whereas the peak intensities change, there are no obvious changes in the wavenumbers of the B–H and N–H stretches of $Al(BH_4)_3{\cdot}6NH_3$ (Figure 4a). This suggests that no interaction exists between $Al(BH_4)_3{\cdot}6NH_3$ and the support; this result is in accordance with the UV measurements (Figure 1d) and our calculations. After heating at 160 °C, the signals that correspond to the BH and NH groups almost disappear in the spectrum of the $Al(BH_4)_3{\cdot}6NH_3$/PSDB composite, while the formation of B–N bonds is observed, which is indicative of B–H/N–H reactions. In contrast, the BH and NH groups can still be detected in bulk $Al(BH_4)_3{\cdot}6NH_3$ at the same temperature. Furthermore, solid-state ^{11}B NMR measurements of the samples obtained at 160 °C (Figure 4b) show that a resonance corresponding to BH_4 was recorded for bulk $Al(BH_4)_3{\cdot}6NH_3$, whereas only the products derived from dihydrogen combination (signals corresponding to BN_3 or BHN_2 and BHN_3 or BN_4 are observable at 19.6 and −0.2 ppm, respectively) are detected in the PSDB-confined material. All of these results confirm a fast consumption of the BH groups of $Al(BH_4)_3{\cdot}6NH_3$ when it is heated within the PSDB resin; dihydrogen interactions were reinforced during the thermolysis process when $Al(BH_4)_3{\cdot}6NH_3$ was incorporated into the PSDB resin. The conversion of BH_4 into a sp^2 boron species in PSDB-confined $Al(BH_4)_3{\cdot}6NH_3$ occurred at lower temperatures than for other MBAs; for those, a temperature greater than 300 °C is required to completely consume the BH groups.[14]

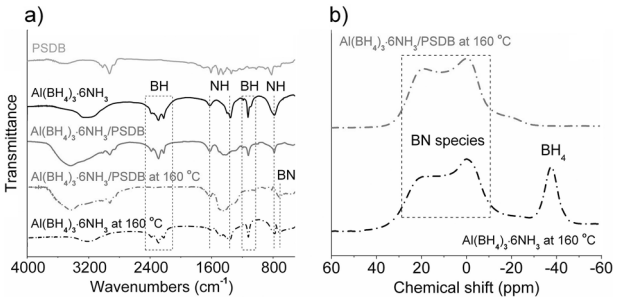

Figure 4. a) FTIR spectra of the PSDB resin, bulk $Al(BH_4)_3{\cdot}6NH_3$, and the $Al(BH_4)_3{\cdot}6NH_3$/PSDB composite, as well as of bulk and PSDB-confined $Al(BH_4)_3{\cdot}6NH_3$ that were heated at 160 °C. b) Solid-state ^{11}B NMR spectra of bulk and PSDB-confined $Al(BH_4)_3{\cdot}6NH_3$ that was heated at 160 °C.

Motivated by recent examples of the use of hydrazine for the regeneration of dehydrogenated residues of B–N based

 © 2013 Wiley-VCH Verlag GmbH & Co. KGaA, Weinheim

hydrides (such as ammonia–borane[15] and lithium amidoborane[16]), we implemented the same approach for $Al(BH_4)_3{\cdot}6NH_3$. After treatment with hydrazine in liquid ammonia, the ^{11}B NMR signals of decomposed residues of $Al(BH_4)_3{\cdot}6NH_3$/PSDB diminished; this was accompanied by the appearance of a broad resonance at 0–30 ppm that corresponds to the superimposition of the BH, BH_2, and BH_3 signals (Figure 5a).[17] This confirms the scission of the B–N

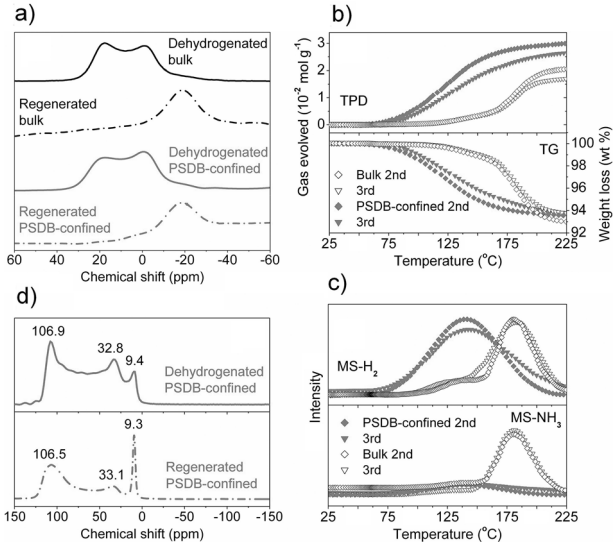

Figure 5. a) Solid-state ^{11}B NMR spectra of the dehydrogenation products of bulk and PSDB-confined $Al(BH_4)_3{\cdot}6NH_3$ before and after the hydrazine-regeneration process; both samples were heated to 225 °C for complete dehydrogenation. b) TPD-TG and c) MS profiles for the samples of bulk $Al(BH_4)_3{\cdot}6NH_3$ and PSDB-confined $Al(BH_4)_3{\cdot}6NH_3$ that were regenerated several times, with a heating rate of 5 °C min^{-1} (PSDB was not considered as a gravimetric component in the measurements). d) Solid-state ^{27}Al NMR spectra of the dehydrogenated products of PSDB-confined $Al(BH_4)_3{\cdot}6NH_3$, before and after the regeneration process.

bonds; subsequently, more hydrogen atoms are attached to the sp^2 boron centers upon the regeneration process, which is in agreement with the FTIR results (Supporting Information, Figure S12). Similar products to those of the bulk material are also observed in the ^{11}B NMR spectra of $Al(BH_4)_3{\cdot}6NH_3$/PSDB before and after the regeneration process.

Calculations with the TPD/TG results (Figure 5b) indicated that the materials that were obtained by the first regeneration of the bulk sample can liberate 3.6 wt% of hydrogen, with a H_2 purity of 90.1 mol% before heating to 225 °C, whereas 6.0 wt% of hydrogen (2.2 wt% relative to the whole system) with a H_2 purity of 99.0 mol% is released from the PSDB-confined material after the first regeneration. Subsequent MS tests (Figure 5c) further demonstrated that ammonia emission is significantly suppressed in the PSDB-confined regenerated material compared with the bulk material. This confirms that the PSDB resin continues to play an important role in enhancing the dehydrogenation performance of the regenerated materials because of its durable size-controlling effect during the regeneration process (Supporting Information, Figure S13).

Elemental analysis of the dehydrogenated product of PSDB-confined $Al(BH_4)_3{\cdot}6NH_3$ gives a composition of $AlB_3N_6H_6$; this corresponds to an approximate H_2 liberation of 14.0 wt% from $Al(BH_4)_3{\cdot}6NH_3$, which is consistent with the TPD result (Supporting Information, Table S1 and Figure S9). Elemental analysis of the product of the first regeneration of PSDB-confined $Al(BH_4)_3{\cdot}6NH_3$ gives the formula $AlB_3N_9H_{22}$. The increased nitrogen content in $AlB_3N_9H_{22}$ may be due to the coordination NH_3 ligands to the aluminum cation during the treatment with liquid ammonia, which results in an excess of NH groups compared to BH groups. This process was further verified by ^{27}Al NMR spectroscopy (Figure 5d). Dehydrogenated $Al(BH_4)_3{\cdot}6NH_3$/PSDB shows a principal signal at 106.9 ppm, along with two signals at 32.8 and 9.4 ppm, which correspond to three-, four-, and six-coordinate Al atoms and are similar to those obtained for dehydrogenated $Al(BH_4)_3{\cdot}6NH_3$.[5a] This observation suggests the cleavage of some Al–N bonds during the dehydrogenation. After regeneration, an enhanced signal that corresponds to a six-coordinate aluminum center is observed,[18] which implies an increase in the number of Al–N bonds. During the thermal decomposition process of $Al(BH_4)_3{\cdot}6NH_3$ incorporated in PSDB, Al–N bond cleavage and formation of N–B networks occurred to yield $AlB_3N_6H_6$. When the regeneration reaction was conducted in liquid ammonia, the aluminum atoms in $AlB_3N_6H_6$ can coordinate to NH_3 to produce more Al–N coordinate bonds, thus yielding $AlB_3N_9H_{22}$.

Although more than half of the amount of hydride was not regenerated from dehydrogenated $Al(BH_4)_3{\cdot}6NH_3$/PSDB, PSDB-confined $Al(BH_4)_3{\cdot}6NH_3$ that had been regenerated twice also had a composition of $AlB_3N_9H_{22}$, as determined by elemental analysis. The capacity (5.7 wt%, corresponding to 2.1 wt% for the system) and purity (98.9 mol%) of the third dehydrogenation from $Al(BH_4)_3{\cdot}6NH_3$/PSDB (Figure 5b) is close to that of the second dehydrogenation (6.0 wt% and 99.0 mol%, respectively). Specifically, 42% and 40% of the initial H_2 release capacity were achieved with the products of the first and the second regeneration, respectively (Supporting Information, Figure S14). This suggests that the new material ($AlB_3N_9H_{22}$) that was obtained by the first dehydrogenation of $Al(BH_4)_3{\cdot}6NH_3$/PSDB is a potentially recyclable hydrogen-storage medium.

In summary, the immobilization of a volatile metal borohydrides by using the phenyl rings of a polymer scaffold to absorb the MB into its porous nanostructure with a good distribution was demonstrated for the first time. We then showed the in situ formation of a metal borohydride ammoniate by treatment with ammonia. The nanosized MBA featured an advanced hydrogen-storage performance well beyond that of its bulk counterpart, PSDB-confined $Al(BH_4)_3{\cdot}6NH_3$. With this material, dehydrogenation with high purity (> 99 mol%) and superior kinetics was achieved. More importantly, dehydrogenated $Al(BH_4)_3{\cdot}6NH_3$/PSDB can be at least partly regenerated, and the rehydrogenated material showed recyclable hydrogen-storage properties. However, to realize full chemical regeneration of $Al(BH_4)_3{\cdot}6NH_3$ from its decomposition products, considerable efforts are still required to overcome inevitable issues,

 © 2013 Wiley-VCH Verlag GmbH & Co. KGaA, Weinheim

including a low yield of regeneration and the energetically demanding hydrazine-based process. Further studies are underway to develop new reductants and optimized regeneration schemes, so that a highly efficient regeneration of MBAs and other B–N-based hydrogen-storage materials may be achieved.

Received: July 12, 2013
Published online: October 2, 2013

Keywords: boron · dehydrogenation · hydrogen · polymers · porous materials

[1] a) L. Schlapbach, A. Züttel, *Nature* **2001**, *414*, 353 – 358; b) A. Züttel, *Mater. Today* **2003**, *6*, 24 – 33.
[2] W. Grochala, P. P. Edwards, *Chem. Rev.* **2004**, *104*, 1283 – 1316.
[3] a) S. Orimo, Y. Nakamori, J. R. Eliseo, A. Züttel, C. M. Jensen, *Chem. Rev.* **2007**, *107*, 4111 – 4132; b) F. H. Stephens, V. Pons, R. T. Baker, *Dalton Trans.* **2007**, 2613 – 2626; c) H. W. Li, Y. Yan, S. Orimo, A. Züttel, C. M. Jensen, *Energies* **2011**, *4*, 185 – 214.
[4] A. Züttel, P. Wenger, S. Rentsch, P. Sudan, P. Mauron, C. Emmenegger, *J. Power Sources* **2003**, *118*, 1 – 7.
[5] a) Y. H. Guo, X. B. Yu, W. W. Sun, D. L. Sun, W. N. Yang, *Angew. Chem.* **2011**, *123*, 1119 – 1123; *Angew. Chem. Int. Ed.* **2011**, *50*, 1087 – 1091; b) Y. H. Guo, H. Wu, W. Zhou, X. B. Yu, *J. Am. Chem. Soc.* **2011**, *133*, 4690 – 4693; c) Q. F. Gu, L. Gao, Y. H. Guo, Y. B. Tan, Z. W. Tang, K. S. Wallwork, F. W. Zhang, X. B. Yu, *Energy Environ. Sci.* **2012**, *5*, 7590 – 7600.
[6] a) Y. Jia, L. N. Cheng, N. Pan, J. Zou, G. Q. Lu, X. D. Yao, *Adv. Energy Mater.* **2011**, *1*, 387 – 393; b) X. Liu, H. W. Langmi, S. D. Beattie, F. F. Azenwi, G. S. McGrady, C. M. Jensen, *J. Am. Chem. Soc.* **2011**, *133*, 15593 – 15597.
[7] a) T. He, Z. Xiong, G. Wu, H. Chu, C. Wu, T. Zhang, P. Chen, *Chem. Mater.* **2009**, *21*, 2315 – 2318; b) T. He, J. Wang, G. Wu, H. Kim, T. Proffen, A. Wu, W. Li, T. Liu, Z. Xiong, C. Wu, H. Chu, J. Guo, T. Autrey, T. Zhang, P. Chen, *Chem. Eur. J.* **2010**, *16*, 12814 – 12817; c) T. He, J. Wang, T. Liu, G. Wu, Z. Xiong, J. Yin, H. Chu, T. Zhang, P. Chen, *Catal. Today* **2011**, *170*, 69 – 75; d) T. J. Frankcombe, *Chem. Rev.* **2012**, *112*, 2164 – 2178.
[8] P. Wang, X. D. Kang, *Dalton Trans.* **2008**, 5400 – 5413.
[9] a) Z. Y. Li, G. S. Zhu, G. Q. Lu, S. L. Qiu, X. D. Yao, *J. Am. Chem. Soc.* **2010**, *132*, 1490 – 1491; b) P. Ngene, R. van den Berg, M. H. W. Verkuijlen, K. P. de Jong, P. E. de Jongh, *Energy Environ. Sci.* **2011**, *4*, 4108 – 4115; c) D.-W. Lim, J. W. Yoon, K. Y. Ryu, M. P. Suh, *Angew. Chem.* **2012**, *124*, 9952 – 9955; *Angew. Chem. Int. Ed.* **2012**, *51*, 9814 – 9817.
[10] a) Z. Wu, M. D. Allendorf, J. C. Grossman, *J. Am. Chem. Soc.* **2009**, *131*, 13918 – 13919; b) P. A. Berseth, A. G. Harter, R. Zidan, A. Blomqvist, C. M. Araujo, R. H. Scheicher, R. Ahuja, P. Jena, *Nano Lett.* **2009**, *9*, 1501 – 1505; c) T. Mueller, G. Ceder, *ACS Nano* **2010**, *4*, 5647 – 5656.
[11] P. Adelhelm, P. E. de Jongh, *J. Mater. Chem.* **2011**, *21*, 2417 – 2427.
[12] a) H. Lehmkuhl, *Angew. Chem.* **1965**, *77*, 623; *Angew. Chem. Int. Ed. Engl.* **1965**, *4*, 600 – 601; b) H. Schmidbaur, R. Nowak, B. Huber, G. Muller, *Polyhedron* **1990**, *9*, 283 – 287; c) M. Schulte, F. P. Gabbai, *Chem. Eur. J.* **2002**, *8*, 3802 – 3807; d) J. Q. Wang, L. Huang, L. Gao, J. H. Zhu, Y. Wang, X. Fan, Z. Zou, *Inorg. Chem. Commun.* **2008**, *11*, 203 – 206.
[13] a) P. H. Bird, M. G. H. Wallbridge, *J. Chem. Soc. A* **1967**, 664 – 669; b) N. A. Bailey, P. H. Bird, M. G. H. Wallbridge, *Inorg. Chem.* **1968**, *7*, 1575 – 1581.
[14] a) W. W. Sun, X. W. Chen, Q. F. Gu, K. S. Wallwork, Y. B. Tan, Z. W. Tang, X. B. Yu, *Chem. Eur. J.* **2012**, *18*, 6825 – 6834; b) F. Yuan, Q. F. Gu, X. W. Chen, Y. B. Tan, Y. H. Guo, X. B. Yu, *Chem. Mater.* **2012**, *24*, 3370 – 3379; c) Z. W. Tang, F. Yuan, Q. F. Gu, Y. B. Tan, X. W. Chen, C. M. Jensen, X. B. Yu, *Acta Mater.* **2013**, *61*, 3110 – 3119.
[15] a) A. D. Sutton, A. K. Burrell, D. A. Dixon, E. B. Garner, J. C. Gordon, T. Nakagawa, K. C. Ott, J. P. Robinson, M. Vasiliu, *Science* **2011**, *331*, 1426; b) Z. W. Tang, H. Chen, X. W. Chen, L. M. Wu, X. B. Yu, *J. Am. Chem. Soc.* **2012**, *134*, 5464 – 5467; c) Z. W. Tang, X. W. Chen, H. Chen, L. M. Wu, X. B. Yu, *Angew. Chem.* **2013**, *125*, 5944 – 5947; *Angew. Chem. Int. Ed.* **2013**, *52*, 5832 – 5835.
[16] Z. W. Tang, Y. B. Tan, X. W. Chen, X. B. Yu, *Chem. Commun.* **2012**, *48*, 9296 – 9298.
[17] a) D. J. Heldebrant, A. Karkamkar, N. J. Hess, M. Bowden, S. Rassat, F. Zheng, K. Rappe, T. Autrey, *Chem. Mater.* **2008**, *20*, 5332 – 5336; b) D. Himmelberger, C. Yoon, M. Bluhm, P. Carroll, L. Sneddon, *J. Am. Chem. Soc.* **2009**, *131*, 14101 – 14110.
[18] J. D. M. Kenneth, E. S. Mark, *Pergamon Materials Series*, *Vol. 6*, Pergamon, Oxford, **2002**.

 © 2013 Wiley-VCH Verlag GmbH & Co. KGaA, Weinheim